Vol.25, November.2015 ISSN 2354-7065

Journal of Ocean, Mechanical and Aerospace

-Science and Engineering-

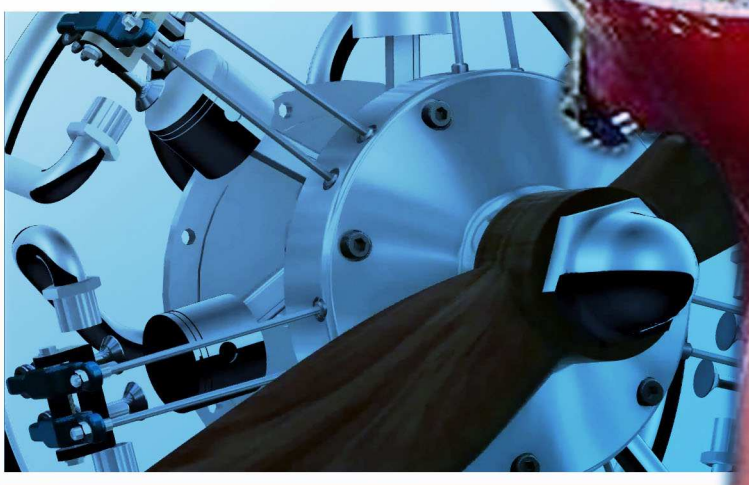

ISOMAse

International Society of Ocean, Mechanical and Aerospace, Scientists and Engineers

Journal of Ocean, Mechanical and Aerospace
-Science and Engineering-
Vol.25: November 30, 2015

Contents

ISOMAse

International Society of Ocean, Mechanical and Aerospace
-Scientists and Engineers-

Journal of Ocean, Mechanical and Aerospace
-Science and Engineering-
Vol.25: November 30, 2015

About JOMAse

The **Journal of Ocean, Mechanical and Aerospace -science and engineering- (JOMAse, ISSN: 2354-7065)** is an online professional journal which is published by the International Society of Ocean, Mechanical and Aerospace -scientists and engineers- (ISOMAse), Insya Allah, twelve volumes in a year. The mission of the JOMAse is to foster free and extremely rapid scientific communication across the world wide community. The JOMAse is an original and peer review article that advance the understanding of both science and engineering and its application to the solution of challenges and complex problems in naval architecture, offshore and subsea, machines and control system, aeronautics, satellite and aerospace. The JOMAse is particularly concerned with the demonstration of applied science and innovative engineering solutions to solve specific industrial problems. Original contributions providing insight into the use of computational fluid dynamic, heat transfer, thermodynamics, experimental and analytical, application of finite element, structural and impact mechanics, stress and strain localization and globalization, metal forming, behaviour and application of advanced materials in ocean and aerospace engineering, robotics and control, tribology, materials processing and corrosion generally from the core of the journal contents are encouraged. Articles preferably should focus on the following aspects: new methods or theory or philosophy innovative practices, critical survey or analysis of a subject or topic, new or latest research findings and critical review or evaluation of new discoveries. The authors are required to confirm that their paper has not been submitted to any other journal in English or any other language.

ISOMAse

International Society of Ocean, Mechanical and Aerospace
-Scientists and Engineers-

Journal of Ocean, Mechanical and Aerospace
-Science and Engineering-
Vol.25: November 30, 2015

Scope of JOMAse

The JOMAse welcomes manuscript submissions from academicians, scholars, and practitioners for possible publication from all over the world that meets the general criteria of significance and educational excellence. The scope of the journal is as follows:

- Environment and Safety
- Renewable Energy
- Naval Architecture and Ship Construction
- Computational and Experimental Mechanics
- Hydrodynamic and Aerodynamics
- Noise and Vibration
- Aeronautics and Satellite
- Engineering Materials and Corrosion
- Fluids Mechanics Engineering
- Stress and Structural Modeling
- Manufacturing and Industrial Engineering
- Robotics and Control
- Heat Transfer and Thermal
- Power Plant Engineering
- Risk and Reliability
- Case studies and Critical reviews

The International Society of Ocean, Mechanical and Aerospace –science and engineering is inviting you to submit your manuscript(s) to admin@isomase.org for publication. Our objective is to inform authors of the decision on their manuscript(s) within 2 weeks of submission. Following acceptance, a paper will normally be published in the next online issue.

ISOMAse

International Society of Ocean, Mechanical and Aerospace
-Scientists and Engineers-

Journal of Ocean, Mechanical and Aerospace
-Science and Engineering-
Vol.25: November 30, 2015

Editors

ISOMAse

International Society of Ocean, Mechanical and Aerospace
-Scientists and Engineers-

Journal of Ocean, Mechanical and Aerospace
-Science and Engineering-, Vol.25

November 30, 2015

Modification and Testing System Control and Swing Model Excavator System

Nazaruddin,[a,*] and Anang Suhandi,[a,]

[a)]*Laboratorium Hidrolik dan Pneumatik, Jurusan Teknik Mesin, Fakultas Teknik, Universitas Riau, Indonesia*

*Corresponding author: nazaruddin.unri@yahoo.com

Paper History

Received: 11-November-2015
Received in revised form: 26-November-2015
Accepted: 30-November-2015

ABSTRACT

One of the heavy equipment that play role in development projects is the excavator. An excavator can perform construction work such as digging, splitting, loading and so on. Laboratory of Hydraulics and Pneumatics Mechanical Engineering Faculty of Engineering, University of Riau has produced a model excavator using pneumatic system, support on a controller box, equipped with buttons setting and motion rotary swing 120^o. The research has modifications control system, remove the control box under the excavator and change to the remote system. The motion rotary swing system has changed from 120^o to 360^o. The purpose is all movements similar in general excavator. The result, excavator model using power 12V DC the control system and compressed air drive pneumatic system. The results of testing control system work to properly, the rotary motion of the swing system 360^o and use electric voltage 7,5V will have speed 13,598 rpm, so swing motion from the excavator model similar in general.

KEY WORDS: *Remote; Swing; Control; Excavator*

1.0 INTRODUCTION

Various activities in heavy equipment when a project the construction is done, whether it is the way, bridge, airport, waterworks, reservoir, dam, port, and buildings. Heavy equipment in a project building having a very important role in terms of the sustainability of the project [2].

Generally, excavator have machine for moving all components, using a hydraulic system, pressurized fluid flowed into actuator to move the arms as boom, stick and bucket, as the technology and found the system excavator to move using motorcycle hydraulic on wheels the chain [9].

Mechanical Engineering Laboratory Hydraulic and Pneumatic of University of Riau has produced a model of excavator [8], by using pneumatic system and taken advantage of pressurized air to move translation and rotation. Its movement is only an arm motion and maximum swing rotation in 120^0. All the movements of the excavator model are controlled by knobs control which is with the excavator. There are two ways to actuate the excavator. Firstly, the excavator moves single cycle where the operator is just depressing single button to actuate the excavator including all of arm components in order to be able in loading and unloading process load with sway motion 120^0 and moving back to original position. Secondly, the excavator is actuated manually by operator with existing control systems. The control system serves as control module to activate all of the components.

2.0 THEORY

2.1 Excavator Definition

The excavator is one of heavy equipment which is consist of components such as boom, arm, bucket, and hydraulic and electric system. The excavator is used in construction and mining area that are used in digging, trenching, loading and unloading operation. The main part of excavator consists of travelling unit and revolving unit as shown in figure 2.1.

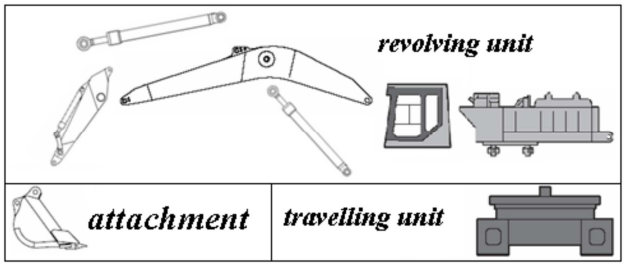

Figure 2.1: Parts of Excavator

2.2 Pneumatic
The Pneumatic is pressurized air which is used in the modern industry to serve a power which is used in remote controlling for a process. [5]. A pneumatic system controlled through with manual and automatic device to activate or to control some equipment.

2.3 Electrical Power
The electric power is associated with a complete electric circuit or circuit component which represent the rate of energy of the moving charges to some other form, e.g., heat, mechanical energy. This energy is stored in electric field or magnetic field. The power of DC Circuit is given by the product of applied voltage and electric current:

$$P = V.I \tag{2.1}$$

Where,
V = *Voltage* (Volt)
P = *Power* (Watt)
I = *Current* (Ampere)

2.3.1 Direct Current
The Direct Current is the unidirectional flow or movement of the electric charges. In general, the direction or movement stays the same time at all time [11].

2.3.2 Direct Current Motor
A Direct current motor represents the electromagnetic field where the electrical energy is converted to the mechanical energy. Furthermore, the mechanical energy is transferred to rotate a shaft.[14]. The rotational speed of the motor can be calculated as follows:

$$V_t = E_a + I_a R_a \tag{2.2}$$

$$E_a = Cn\Phi \tag{2.3}$$

$$\omega = \frac{V_t - I_a R_a}{C\Phi} \tag{2.4}$$

$$\omega = \frac{2\pi n}{60} \tag{2.5}$$

Where:

V_a = input voltage
R_a= Resistance of Winding armature
I_a = Current of armature
E_a= Power of electric in watt
Φ = Magnetic flux in Weber
ω = Angular velocity, Rad/Sec
C = Constanta
n = Revolution per minute (RPM)

2.4 Control System
A control system is sets of devices, which functioned to manage, command is used in the industrial equipment (Fig. 2.2). Physically, the control system is allowed to control the equipment automatically [12].

Figure 2.2: Control System

2.4.1 On-Off Control
The control element has two positions either it is fully closed or fully open. The control system made for such controlling element, is known as on-off control theory.

2.5 Chain
A chain is a series of connected link which consists of one or two more links. The chain is used to transmit the power between two shafts. There are two styles of chain, according to their intended use, namely roll chain and gear chain.

2.5.1 Roll Chain Selection
The horsepower rating is transmitted through roll chain could be calculated as below:

$$HP\ Design = HP \times SF \tag{2.6}$$

where:
$HP\ Design$= Horse Power design
HP = Horse Power of motor
SF = Service Factor as show in table 2.1

Table 2.1: Service Factor

Class of Driven Load	Type of Input Power		
	Internal Combustion Engine with Hydraulic Drive	Electric Motor or Turbine	Internal Combustion Engine with Mechanical Drive
Uniform	1	1	1.2
Moderate	1.2	1.3	1.4
Heavy	1.4	1.5	1.7

Figure 2.3 is used to determine the selected chain number according to the drive sprocket revolution, the transmitted power and the number of chain that will be used.

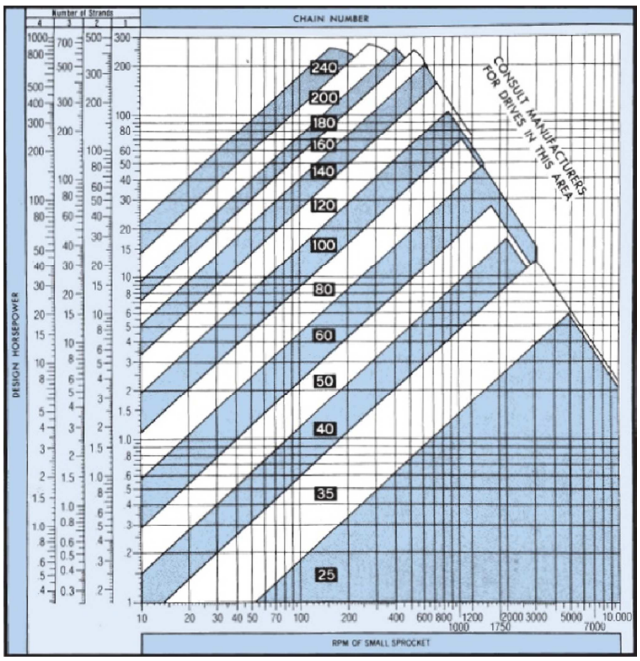

Figure 2.3: Quick Selector Chart

In order to determine the number of strand that will be used in this project, refer to table 2.2

Table 2.2: Number of Strand

No. of Strands	1	2	3	4	5	6
Factor	1	1.7	2.5	3.3	3.9	4.6

The specification of chain number is selected according to Figure 2.3 Standard ASME B29.1M-1993.

The sprocket rotation could be calculated by the equation (2.7) as below:

$$\frac{N_1}{N_2} = \frac{T_2}{T_1} \qquad (2.7)$$

Where,
N_1 = Drive sprocket rotation in rpm
N_2 = Driven sprocket rotation in rpm
T_2 = Number of teeth for drive sprocket
T_1 = Number of teeth for driven sprocket

The chain length is determined by the equation (2.8) as follows:

$$L = K.p \qquad (2.8)$$

Chain link, K is the number of links could be determined by the equation (2.9):

$$K = \frac{T_1+T_2}{2} + \frac{2x}{p} + \left(\frac{T_2-T_1}{2\pi}\right)^2 \frac{p}{x} \qquad (2.9)$$

The sprocket axis distance could be formulated by the equation (2.10) as follows:

$$x = \frac{2T_1+T_2}{6} \qquad (2.10)$$

Where:
L = Length of Chain (mm)
K = Chain Link
p = Pitch (mm)
x = Axis distance between sprockets (mm).

Therefore, the power could be transmitted to satisfy the equation as below:

$$P = \frac{T2\pi N}{60} \qquad (2.11)$$

3.0 METHODOLOGY

The research will be accomplished in three stages. First, Modification of system control. Second, Designing process and manufacturing of the swing system. Third, testing on control system and swing system.

3.1 Modification of System Control

This research is carried out to modify the control system by using the remote control to activate the prototype equipment.

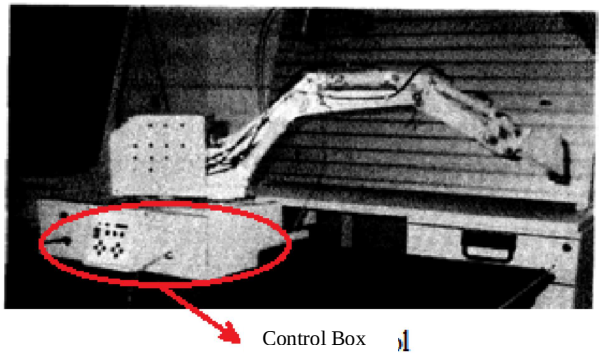

Figure 3.1: Model Excavtor

The flow chart of this research as follows:

No. of Strands	1	2	3	4	5	6

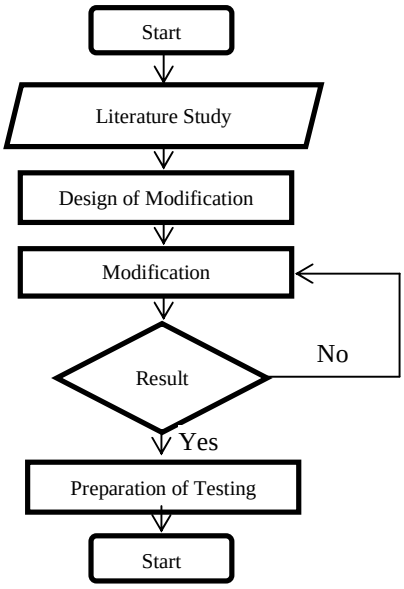

Figure 3.2: Flowchart of Control System Modification

3.1.1 Design of Control System

Design of control system could be seen in figure 3.3

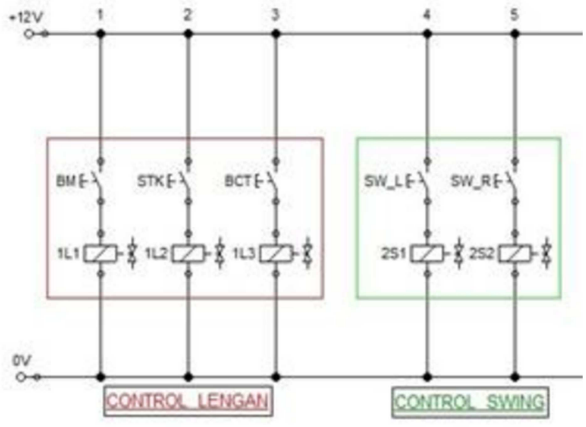

Figure 3.3: Design of electro pneumatic control system

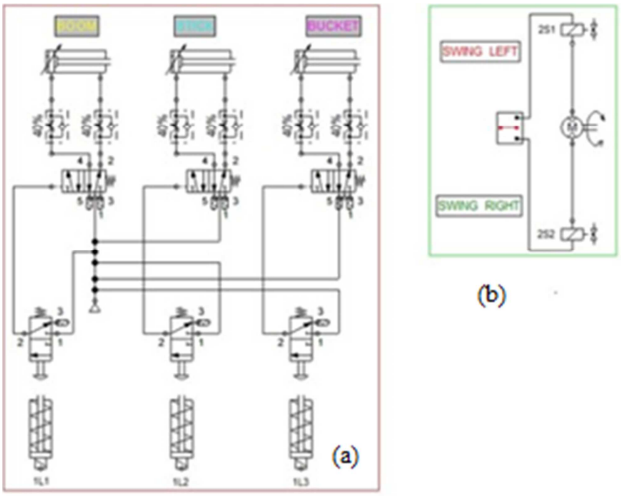

Figure 3.4: Circuit of pneumatic control (a) and circuit of swing (b) from model of excavator

In the circuit consists of pneumatic control system (boom, arm and bucket) and swing control system. Some label in Figure 3.3 and Figure 3.4 is explained as shown in table 3.1

Tabel 3.1: Description of Circuit Control

Label	Description
BM	Button to activate boom
SKT	Button to activate stick
BCT	Button to activate bucket
SW_L	Button to activate swing motor with CW rotation
SW_R	Button to activate swing motor with CCW rotation
1L1	Boom connector socket to Panel Control
1L2	Stick connector socket to panel control
1L3	Bucket connector socket to control panel
2S1	Swing motor connector socket with CW rotation
2S2	Swing motor connector socket with CCW rotation
0V	Input of Power Supply
+12V	Input of Power Supply

3.1.2 Build and Assembly Remote Control

The remote control comprises the several of part component which need to be assembled and joined with electrical cable to transmit the electrical voltage that used to activate all of part of excavator model.

Result of all of the control system can be seen in Figure 3.4 as below.

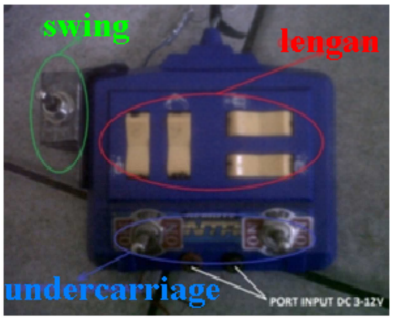

Figure 3.4 Remote Control Assembling

3.2 Swing modification

The old system [8] used in swing control is sliding shaft to rotate the swing (Fig. 3.5). In this study, the electric motor is applied to rotate the swing so the angular movement reach 360 ^{0}, as shown in Fig. 3.6.

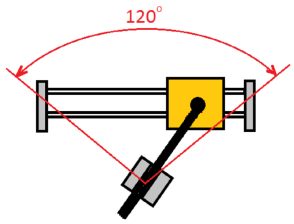

Figure 3.5 Mode swing at the old model

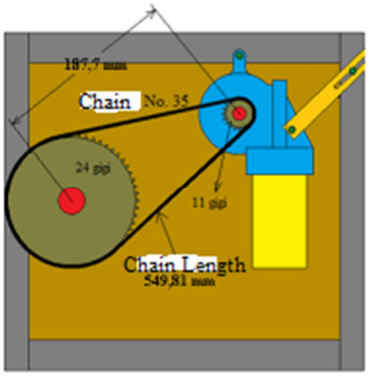

Figure 3.6 Chain and driving system on a new model

4. RESULT

Either of table and figure respectively are shown on Fig. 4.1 (a) and (b) as a final result that had been obtained after modification model of excavator [8].

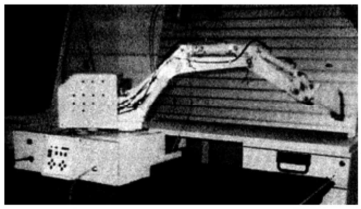
(a). Before Modification


(b). After Modification

Table 4.1: Several state before/after modification

Before Modification	After Modification
Control system is on the box	Part of controlling was placed on a remote and used a wire to connect with system.
Excavator can't move cause have a controlling box under it.	Excavator can make a good travelling by undercarriage.
Old model can make a swing mode only 120^{o} by sliding beam.	New model can do a 360o swing mode was used electric motor and chain transmission.
Position of panel control at the box behind of arms	Panel control had been put at the small box beside an arms.
Serial of pneumatic have been placed on a test table	Serial of pneumatic have been placed behind an arms.

5. CONCLUSION

From step in this research such as design, manufacture and assembly several things are concluded;

1. This study continues previous work to make a remote and modification type of system control become an acting two position on or off.

2. Low voltage can reduce a power that make electric actuator weak. Consequently will be met a little bit time before pneumatic valve pushed a arm.

3. This study had been made a swing system using chain and bicycle sprocket that are driven by electric motor YB037001A from a car power window. The system rotate in 40.882 rpm in voltage 12 V.

4. Revolution on swing can be synchronize with the normally excavator while using 7.5 V and rotate in 13.598 rpm.

REFERENCE

1. Anonim. 2013. *Volvo Construction Equipment*. North America.
2. Ayu, W. Ade. 2007. *Peranan Penting Alat Berat pada Pembangunan JalanTol*. PoliteknikNegeriJakarta.
3. Norberg.C. B. 1993. Presision Power Transmission Roller Chains ASME B29.1M. NewYork, N.Y.
4. Dorf, R.C. 1983. *Sistem Pengaturan Edisi 3*. Jakarta: Erlangga.

5. Ebel F, 2002. *Electropneumatics Festo Didactic Vol 1*. Germany: Festo Didactic Industries.
6. Gustriansyah, Yogi. 2011. Hubungan AntaraTegangan dan RPM Pada Motor Listrik. TeknikElektro ITB.
7. Jeffrey, Renold. 2011. *Roller Drive Chain Selection*. America: Advancing Chain Technology Ltd.
8. Julianto, Nazarudin. 2004. *Perencanaan dan Pengujian Model Excavator*. Paper work. Mechanical Engineering.Universitas Riau.
9. Spotts.M. F. 1964. *Design of Machine Elements*. Northwestern University. Prentice-Hall.
10. Pakpahan, Sahat. 1988. *Kontrol Otomatik Teori dan Penerapan*. Jakarta.Erlangga.
11. Zuhal. 1991. *Dasar Tenaga Listrik dan Elektronika Daya*. Jakarta. PT. GramediaPustaka.

Journal of Ocean, Mechanical and Aerospace
-Science and Engineering-, Vol.25

November 30, 2015

Analysis of Design for Assembly (DFA) in Waste Separation Machine of Ferromagnetic and Non-Ferromagnetic Material

Dodi Sofyan Arief [a,*], Rifki Ilyandi [a,*], Tekad Indra Pradana Abidin [b,*], Amir Hamzah [c,*]

[a)] *Production Technology Laboratory, Department of Mechanical Engineering, Faculty of Engineering, Universitas Riau, Indonesia*
[b)] *PT. Riau Solusi Teknik, Riau, Indonesia*
[c)] *Department of Electrical Engineering, Faculty of Engineering, Universitas Riau, Indonesia*

*Corresponding author: dodidarul@yahoo.com, rifkyilyandi@gmail.com, tekad.abidin@gmail.com, amirhzh.ur@gmail.com.

Paper History

Received: 11-November-2015
Received in revised form: 26-November-2015
Accepted: 30-November-2015

ABSTRACT

Design for Assembly (DFA) is one of method in the assembly systems to ease the assembly during simultaneous process from the beginning until become new products of the whole components. However, the obstacles in assembly process could be occurred in waste separation machine. Therefore, in order to obtain the optimization of assembly process, it is needed to conduct an analysis of component design before the production. DFA analysis will obtain the value of assembly efficiency. The efficiency value of prototype machine will achieve a way to separate the waste, both ferromagnetic and non-ferromagnetic materials. Furthermore, efficiency value theoretically on assembly of waste separation machine is 14.22% at 548.47seconds. The efficiency value of waste separation machine after assembly process in actual condition is 11.83% at 658.88seconds. The distinction efficiency value is caused by difficulties in assembly of the belt roller and sub assembly of base support on motor. As consequences, the time to get assembly will take more time on actual condition rather than theoretically.

KEY WORDS: *Design for Assembly* (DFA), *Efficiency of Assembly*

1.0 INTRODUCTION

Design for Assembly (DFA) is a method to optimize the assembling process in order to obtain the effective cost and to reduce the number of component. Prior to design the assembly process, it is needed to propose a model, drawing or prototype of the assembly.

2.0 THEORY

2.1 Assembling

Assembling is a process to join a component or sub-component to form the product. Types of Assembling divided into:

1. Manual Assembly
   Manual assembly is an assembly process by using man power to assemble a component or sub-component conventionally.
2. Automated Assembly
   Automated assembly refers to the use of programmed machines and automated devices to carry out the various assembly tasks in an assembly process. The vast majority of automated assembly systems are designed to perform a fixed sequence of assembly steps on a specific product.

2.2 Design for Assembly (DFA)

Design for Assembly (DFA) is a method to assemble component and sub-component to form a product in order to optimize the cost efficiency. The manual assembly process could be classified into:

2.2.1 Manual Handling

In a manufacture, the manual handling is an operation of moving part by using hand, arms or some other forms of bodily effort. There are some effects in the process of manual handling such as:
1. Effect of Part Symmetry On Handling Time
Figure 2.1 shows rotational symmetry of part component which is perpendicular to the axis (α) and parallel to the insertion axis (β).

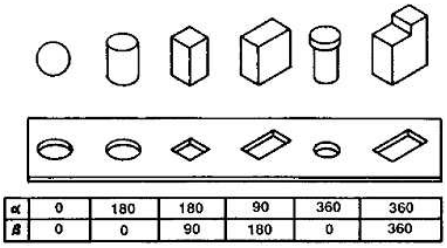

α	0	180	180	90	360	360
β	0	0	90	180	0	360

Figure 2.1: Rotational Symetry of several parts

2. Effect Of Part Thickness and Size On Handling Time.

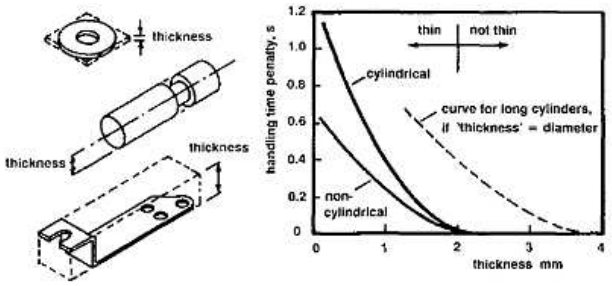

Figure 2.2: Thickness effect

In the figure 2.2 shows the thickness effect to manual handling time in cylindrical and non-cylindrical geometry in assembling process.

3. Effect of Part Size

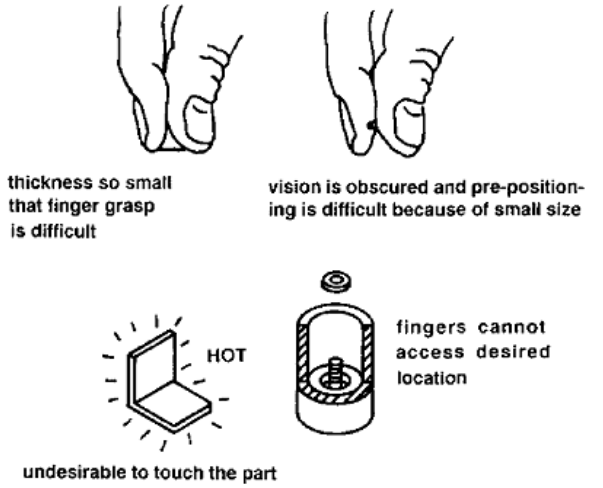

Figure 2.3: Effect of size in manual handling

In the figure 2.3 shows the difficulties of small part in manual handling which can take much time in assembling process.

2.2.2 Manual Insertion

The factors which could affect the time of manual insertion consist of:

1. Effect of Chamfer Design on Insertion Operations.

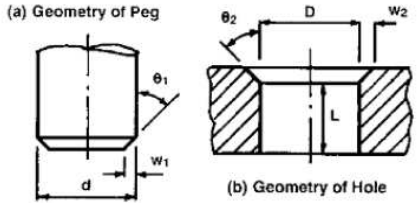

Figure 2.4: Peg and Hole geometry

Figure 2.4 shows the assembly process of two geometries in different chamfer position as shown in figure 2.4 (a) the chamfer in the peg and figure 2.4 (b) the chamfer on edge of geometry.

2. Effect Of Holding Down

This condition can be defined as holding in certain time in order to wait the sequence process of assembly.

2.2.3 Boothroyd-Dewhusrt Table Matrices

Boothroyd-Dewhusrt performed some experiments to identify the resistances and difficulties of assembly process. The combination of them was tabulated which refers to Table 3.2 and Table 3.3.

2.2.4 Assembling Efficiency

The assembling efficiency of product could be calculated as follow:

$$E_{ma} = \frac{N_{min} t_a}{t_{ma}} \quad (2.1)$$

Where,

N_{min} =Theoretical minimum number of parts
t_a = Basic assembly time for one part (3s)
t_{ma} = Estimated time to complete

3.0 METHOD

3.1 Flowchart

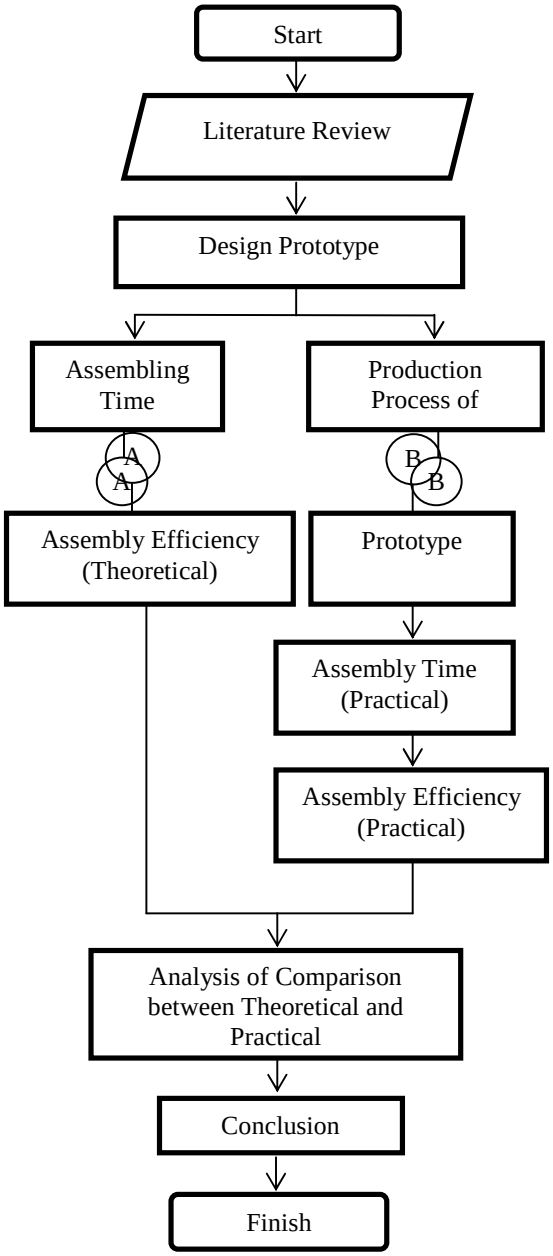

Figure 3.1: Flowchart of research

3.1.1 Theoretical Time estimation

The estimation of Assembling Time theoretically can be seen in the flowchart below:

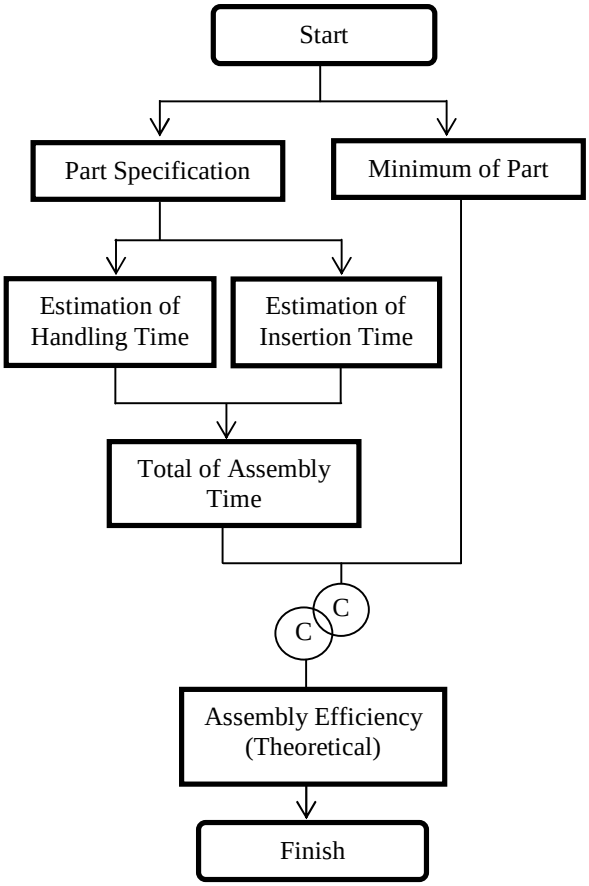

Figure 3.2: Estimation of Assembly Time in theoretical

Table 3.1 explains how to determine the estimation of assembling time per part of unit. Afterward, the assembling time of each part will be inserted to the worksheet analysis table.

Table 3.1: Worksheet Analysis

Items Name	*Number of item (RP)*	*Handling Code*	*Handling Time (TH)*	*Insertion Code*	*Insertion Time (TI)*	*Total Time (s) (RP)*(TH+TI)*	*Min. Part*	
Total								

The items of worksheet analysis can be explained as follow:

a. Number of items (RP) is the number of same part unit.
b. Handling code consists of two-digit of number which is used to determine the handling time according to Table 3.2 Estimation of handling time.
c. Handling Time (HT) is the required time to handle the part.
d. Insertion Code is two-digit number to determine the handling time of insertion according to the Table 3.3 estimation of handling time.
e. Insertion Time is the required time to joint each of part that needed to be assembled.
f. Total Time is number of item (RP) which is multiplied by increment of handling time and insertion time.
g. Minimum Part is one of the important parameter to determine assembly efficiency.

3.1.2 Estimation of Assembly Time in Practice

After the prototype of products was complete, the next step is preparing the assembly process in order to take the required time to establish the product. The assembly process involves five operators to assemble the machine. Each of operator assigned three times of assembly process in rotation, and each of assembly process run along with stopwatch to count the time taken. The process of required time in assembling can be described by flowchart below:

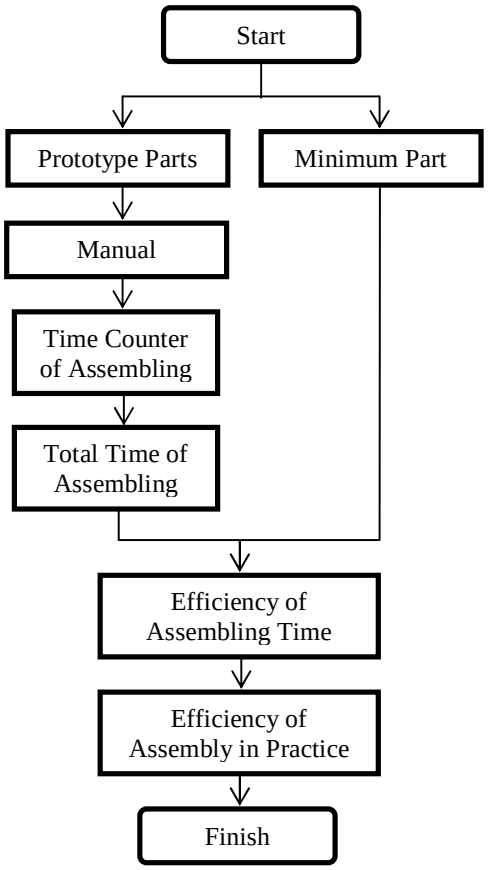

Figure 3.3: Flowchart of Assembly Time in Practice

3.2 Material of Research

In this research, the design of waste separation machine is showed in Figure 3.4 (a) and the prototype showed in Figure 3.4 (b).

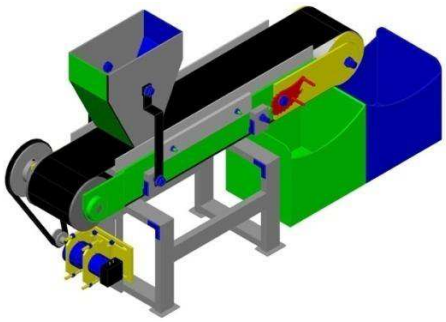

Figure 3.4: (a) Design of waste separation machine.

Figure 3.4 (b): Prototype of waste separation machine

4.0 THE RESULT OF ESTIMATION TIME AND EFFICIENCY

Table 4.1 shows the result of estimation time (t_{ma}) and efficiency either in theoretical or practical. Based on the theory, the total time of assembly to all components is 548.47second and the value of assembly efficiency is 14.22 %. Whereas in practical, the total time of assembly to all of component is 658.88second and the value of assembly efficiency is 11.83 %.

Table 4.1: The Result of assembling time estimation

Items Name	Number of item (RP)	Handling Code	Handling Time (TH)	Insertion Code	Insertion Time (TI)	Total Time (s) (RP)*(TH+TI)	Min. Part
1.Body Mounting	1	93	3	-	0	3	0
2. Body	1	93	3	7	6.5	9.5	0
3.Body Bolt	4	10	1.5	6	5.5	28	0
4.Body Nut	4	1	1.8	38	6	31.2	0
5.Rear Bearing Roller	2	0	1.13	7	6.5	15.26	2
6.Rear Roller	1	10	1.5	6	5.5	7	1
7.Rear Roller Arm	1	30	1.95	6	5.5	7.45	1
8.Rear bolt arm	3	10	1.5	6	5.5	21	0
9.Rear nut arm	3	0	1.5	38	6	22.5	0
10.Pulley 4.5”	1	10	1.5	6	5.5	7	1
11.Magnet-steel	1	15	2.25	2	2.5	4.75	1
12.Front roller cover left hand side	1	10	1.8	8	6.5	8.3	1
13.Front roller	20	1.8	2	2.5	4.3	1	20
14.Front roller cover right han side	1	10	1.8	8	6.5	8.3	1
15.Front bearing	2	0	1.13	7	6.5	15.26	2
16.Bushing	2	0	1.13	0	1.5	5.26	0
17.Front roller arm	2	30	1.95	6	5.5	14.9	0
18.Front shaft ring	2	3	1.69	0	1.5	6.38	0
19.Front shat nut	2	0	1.13	38	6	14.26	0
20.Belt tensioner shaft ring	2	3	1.69	0	1.5	6.38	0
21.Belt tensioner	2	30	1.95	0	1.5	6.9	2
22.Hollow shaft	1	0	1.13	6	5.5	6.63	
23.Adjuster shaft	1	0	1.13	6	5.5	6.63	1
24.Adjuster shaft nut	1	0	1.13	38	6	7.13	0
25.Front Sub-assembly roller	1	95	4	98	7	11	0
26.Belt bracket	1	20	1.8	1	2.5	4.3	1
27.Belt roller	1	80	4.1	32	4	8.1	1
28.Belt stopper	2	30	1.95	6	5.5	14.9	2
29.Belt stopper nut	4	10	1.5	38	6	30	4
30.DC motor	1	10	1.5	0	1.5	3	1
31.Bracket motor	2	20	1.8	6	5.5	14.6	
32.Motor bracket nut	4	10	1.5	38	6	30	
33.Motor belt	1	0	1.13	0	1.5	2.63	1
34.Motor mounting	1	30	1.95	7	6.5	8.45	1
35.Motor mounting bolt	4	10	1.5	7	6.5	32	0
36.Motor mounting nut	4	10	1.5	58	10	46	0
37.Inlet arm	2	30	1.95	6	5.5	14.9	2
38.Underneath inlet arm nut	2	10	1.5	38	6	15	0
39.Inlet	1	20	1.8	6	5.5	7.3	1
40.Inlet bolt	2	10	1.5	0	1.5	6	2
41.Inlet nut	2	10	1.5	38	6	15	0
42.Adjusting belt roller	1	-	-	98	9	9	0
43.Adjusting belt motor	1	-	-	98	9	9	0
TOTAL						548.47	26

5.0 DISCUSSION

The assembly process obtained the difference between theoretical assembly efficiency and in practical. In theoretical, it resulted 14.22% and in practical, it resulted 11.83%. So the difference is 2.39%. This condition indicates the assembly process in practical is faster than estimation time in theoretical because of some part can be assembled in the same time during the assembly process

which can save the time in the same result. The assembly process is showed in Figure 5.1 and 5.2.

Figure 5.1: Assembly of belt roller.

Figure 5.2: Assembly of Motor Mounting

6.0 CONCLUSION

The assembly efficiency in practical is less than theoretical. Based on Design for Assembly (DFA), it indicates that the assembly time can be short and also reduce the cost of assembly.

REFERENCE

1. Boothroyd, G. 2005. *Assembly Automation and Product design*. Second Edition. Wakefield.
2. Dekker M, 2002. *Manufacturing Engineering And Materials Processing*. Marcel Dekker Inc. New York.
3. Kristyanto dan Dewa SP, 1999. Kontribusi Ergonomi untuk Rancangan Perakitan. Jurnal Teknologi Industri 3(1) : 47-62.
4. Suhdi,2009. Teori Dasar Perakitan. http://suhdi. wordpress.com/2009/01/31/teori-dasar-perakitan/. diakses pada 12 Juni 2014.
5. Yusri, 2008. Penerapan Design for Assembly (DFA) untuk mereduksi biaya produksi suatu produk, Politeknik Negeri Padang.

Journal of Ocean, Mechanical and Aerospace
-Science and Engineering-, Vol.25

November 30, 2015

Evaluation of Mechanical Properties and Wear Behavior of Aluminium-Red Mud Composite Synthesized By Powder Metallurgy

Neelima Devi Chinta,[a,*] N. Selvaraj,[b] and V. Mahesh[c]

[a)]*Department of ME, University College of Engineering, JNTUK, Vizianagaram -535003, India.*
[b)]*Department of ME, National Institute of Technology, Warangal - 506004, India.*
c)Department of ME, S.R Engineering College, Warangal - 506371, India.

*Corresponding author:Neelima Devi Chinta, Email: cneelima.me@jntukucev.ac.in

Paper History

Received: 14-November-2015
Received in revised form: 29-November-2015
Accepted: 30-November-2015

ABSTRACT

Red mud received from NALCO, Odisha, India has been subjected for sieve analysis and milled to 42 nanometers using high energy ball mill. Pure aluminium powder of 99.72% purity as matrix with red mud as reinforcement at 2%, 4%, and 6% weight fractions at micro as well as nano levels. Micro and nano structured red mud powders and pure aluminium are mixed in a V-blender, compacted at a pressure of 40 bar and samples are prepared by conventional sintering. The mechanical properties of Aluminium-Red mud micro and nano composites are evaluated with respect to hardness and compression strength. The experimental compression strength values are validated by Deform-2D software. An increase in hardness and compression strength is observed with increase in the amount of percentage weight fraction of Red mud. Wear characteristics are investigated using pin-on-disc wear testing machine and evaluated the prediction of optimal combination of pure aluminium and weight fraction of micro and nano structured red mud powder using Regression analysis. Highest wear resistance is observed for the test specimen with 42 nm size and 6% weight fraction of red mud powder at 600 RPM speed.

KEY WORDS: *Nanocomposites; Sintering and Mechanical Properties.*

NOMENCLATURE

Al	Aluminium
RM	Red mud
Φ	Diameter
%	Percentage

1.0 INTRODUCTION

Red mud is an industrial solid waste which is known as bauxite residue obtained during the processing of alumina by Bayer's process. An attempt has been made to utilize this solid waste using as the reinforcement material in Metal Matrix Composites (MMCs) and Metal Matrix Nano Composites (MMNCs). A lot of difficulty is being experienced by the manufacturing industries to dispose their wastage and utilize their byproducts. The Bauxite residue which is known as Red mud is mixed with other metals mainly to aluminum to form metal matrix composites which exhibit superior mechanical properties and applications [1, 2]. Powder compaction is the process of compacting metal powder in a die through the application of high pressures. The powder is compacted into a shape using the punch tool held in vertical orientation and then ejected from the die cavity. Hazardous industrial, electronic, and bio medical wastes lead to burden on the earth [3, 4]. Hence waste treatment is one of the top most problems of the world. Red mud has been used in the removal of Sulphur compounds from kerosene oil [5, 6], in the heap leaching of gold ores as a pH modifier [7, 8], in the anthracene hydrogenation [9, 10] and as a pigment in marine paints as anticorrosive [11, 12, 13].

In China, approximately 10% of Red mud produced is recycled for further metal extraction or utilized as a raw material for brick production [14]. In India, it is reported that 2.5 million

tons are absorbed by the cement industry. Residual Bauxite was introduced as a raw material along with other raw materials such as lime, clay, silica etc. The tests confirmed that residue added cement, as well as mortar and concrete made from this cement, meet the Japanese Industrial Standards [15].

2.0 EXPERIMENTAL SET UP

2.1 Sieve analysis

Sieve analysis (or gradation test) is a procedure used to assess the particle size distribution of a granular material. It is also called as particle sizing technique. The red mud used for the present investigation is collected from the National Aluminum Company Limited (NALCO) Damanjodi, Odisha, India. The Chemical compositions of Red mud and Pure Aluminium powder of 99.72% purity are shown in Table 1 and 2 respectively.

Table 1: Chemical composition of Red mud

Fe_2O_3	Al_2O_3	TiO_2	SiO_2	Na_2O	CaO	V_2O_5	Others
53.8	14.3	3.9	8.34	4.3	2.5	0.38	Balance

Table 2: Chemical composition of Pure Aluminium

Element	Fe	Si	Mg	Mn	Cu	Zn
Wt%	0.17	0.07	0.001	0.0008	0.005	0.003

As-received Red mud is subjected to sieve analysis using mechanical sieve shaker for collecting particles of uniform sizes of 100, 150, and 200 microns for preparing the micro sized Red mud powder.

2.2 High Energy Ball Milling

Nano particles are formed in a mechanical device known as high energy ball mill referred to as Pulverisette for conducting mechanical attrition experiments. The reduction in particle size of Red mud from micron level to the nano level is carried out using a high-energy planetary ball mill in a stainless steel chamber using tungsten carbide of 10 mm Φ size. The micron sized Red mud powder is milled for 30 hours by maintaining the rotation speed of the planet carrier at 200 rpm. The ball mill is loaded with ball to powder weight ratio (BPR) of 10:1. Toluene is used as the medium with an anionic surface active agent to avoid agglomeration. The milled sample powder is taken out after 6 hours, 13 hours, 24 hours and 30 hours of milling and dried with mechanical drier. The XRD Pattern for 30 hours milled Red mud is shown in figure 1.

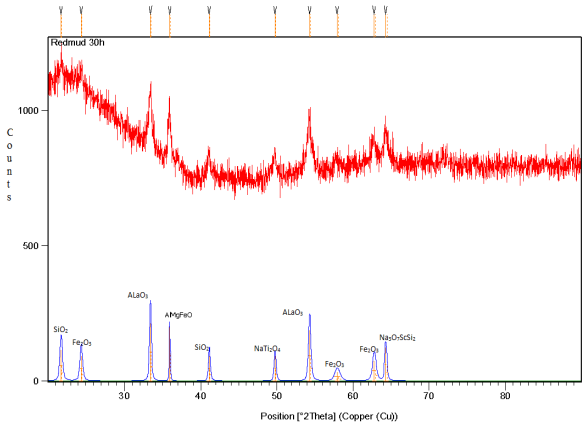

Figure 1: XRD Pattern for 30 hours milled Red mud.

The crystallite size is reduced from 400 nm to 42 nm during 30 hours of ball milling. The fresh Red mud powder particles are mostly angular in shape. The shapes of the 30 hours milled particles are irregular and the surface morphology is rough. The relative lattice strain is increasing with increasing the duration of milling time. This lattice strain is increased from 0.12 to 0.28 for as-received Red mud powder after 30 hours of milling. The intensity of the peaks in the XRD pattern got reduced and the peak broadening increased as the duration of milling time increases.

2.3 Mixing and Compacting

The micro level Red mud powders of 100, 150 and 200 microns and nano level Red mud powder of 42 nm (or 0.042 microns) at 2%, 4% and 6% of weight fractions are mixed with Pure Aluminium powder in a double cone mixer for 10 hours in order to obtain proper interaction of particles with each other. The different proportions of Al-Red mud sample materials are compacted in a hydraulic press of 100 ton load capacity and 7.5 H.P. During compacting pressure applied was 40 bar and compact pressing time was 4 sec.

2.4 Sintering

Sintering is a thermal treatment, below the melting temperature of the main constituent material, which transforms a metallic or ceramic powder (or a powder compact) into a bulk material. The Vacuum maintained during sintering was 250 Pa (using a compressor of 1.5 H.P) and raising the temperature to 300^0C in 30 minutes soaking at 300^0C for 30 minutes. Then raising the temperature to 620^0C(time taken is 35minutes) and again soaking at 620^0C for 30 minutes. Then cooling is done to room temperature (time taken is about 3hrs). Hence the total sintering cycle time was 5hours 5minutes.

Figure 2: Compacted Pure Aluminium and Red mud samples in Sintering Machine.

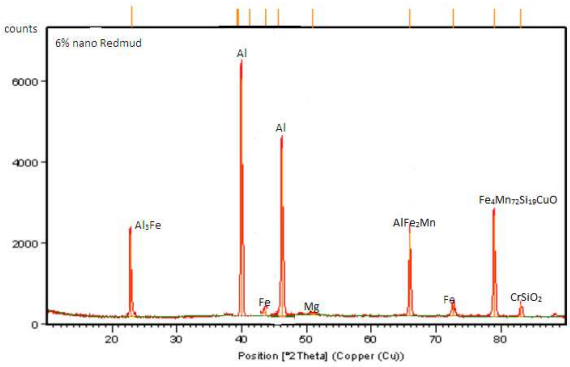

Figure 3: XRD pattern for Pure Aluminium and 6% nano Red mud compacted sample after Sintering.

Table 3: Hardness values for Aluminium with Redmud samples

S.No	Specimen composition	Vickers Hardness Number
1	Pure Al (99.72% purity)	47.4
2	Al with 2% Red mud (100 microns)	60.2
3	Al with 4% Red mud (100 microns)	67.6
,	Al with 6% Red mud (100 microns)	74.5
5	Al with 2% Red mud (150 microns)	58.3
6	Al with 4% Red mud (150 microns)	62.4
7	Al with 6% Red mud (150 microns)	69.2
8	Al with 2% Red mud (200 microns)	56.7
9	Al with 4% Red mud (200 microns)	59.3
10	Al with 6% Red mud (200 microns)	63.5
11	Al with 2% Red mud(0.042 microns)	73.6
12	Al with 4% Red mud(0.042 microns)	77.4
13	Al with 6% Red mud (0.042microns)	83.9

The figure 2 shows the Aluminium and Red mud compacted samples in Sintering Machine of vacuum chamber. The Vacuum sinter furnace is manufactured by ACME (Advanced Corporation for Materials and Equipments), China. The Model No. ZSJ-25x25x50 with loaded weight of 50 kg and loaded vacuum of $4x10^{-3}$ Pa. The raised sintering furnace temperature upto 1550^0C with heating power capacity of 50kW. The Figure 3 shows the X-Ray Diffraction (XRD) pattern for Pure Aluminium and 6% nano Red mud compacted sample which has Al-Al_3Fe phase and many other compounds like $AlFe_2Mn$, $Fe_4Mn_{72}Si_{19}CuO$, Mg after Sintering. This confirms the presence of Red mud in the pure Aluminium powder based nano metal matrix composite. There are nine peaks have been obtainted in the 2θ span ranging from 10 to 100. The micro Vickers Hardness values for pure Aluminium and Aluminium with Redmud are shown in Table 3.

3.0 RESULTS AND DISCUSSIONS

3.1 Hardness and Compressive strength

Hardness values are measured using Micro Vickers Hardness tester. The graph between Hardness and % weight fraction of Red mud is shown in figure 4. Aluminium is a ductile material, addition of small amount of reinforcement material to it will gives strength but not change its ductility so compression strength at 10, 20, and 30 percent reduction is determined. Using Compression Testing machine Compression Strength values are calculated experimentally and validated using Deform-2D software.

The figure 5 shows compressive stress for 100 microns with particle size of 6% weight fraction of Red mud with Pure Aluminium at 10% reduction using Deform-2D software. Both experimental and Deform-2D simulated compressive stress values are shown in Table 4 and Table 5 respectively.

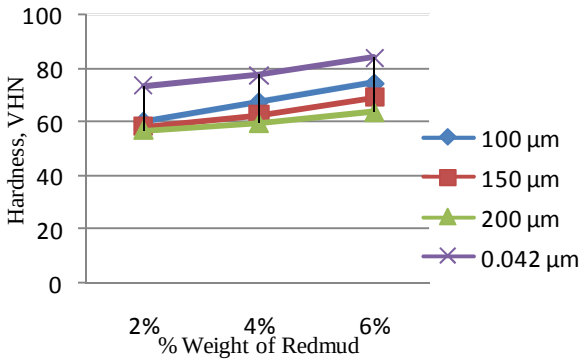

Figure 4: Plot between Hardness and % Weight fraction of Red mud.

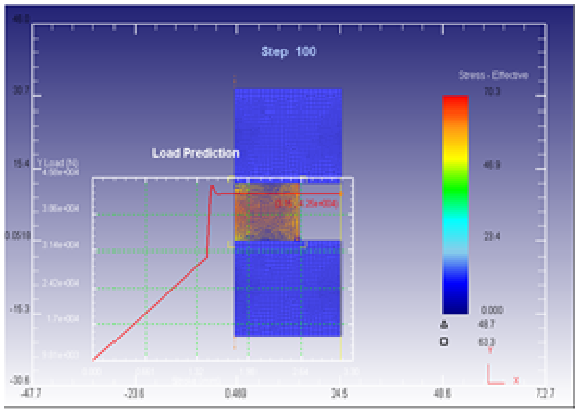

Figure 5: Compressive Stress for Pure Aluminium with 6% weight fraction of Red mud of 100 microns size at 10% reduction.

Table 4: Experimental results of Compressive Strength from Deform-2D software

S.No	%Wt of Red mud	Particle size μ m	Stress at 10% reduction MPa	Stress at 20% reduction MPa	Stress at 30% reduction MPa
1	Pure Aluminium	45	53.7	70.7	79.5
2	Aluminium + 2%RM	100	48.9	75.2	81.5
3	Aluminium +2% RM	0.042	49.9	77.1	82.4
4	Aluminium +4% RM	100	51.4	80.8	87.8
5	Aluminium +4% RM	0.042	62.3	76.4	89.6
6	Aluminium +6% RM	100	70.3	89.7	94.6
7	Aluminium +6% RM	0.042	58.2	92.1	98.4

Hardness and Compression Strength values are depicted the information that Nano Red mud specimens have more hardness and compression strength when compared with micro nature specimens. As % weight fraction composition of Red mud increases, hardness and Compression Strength values are also increases. This is due to the ferrous materials are harder in nature. Since the Red mud consists of ferrous oxide as its major constituent about 53.8%. Hence this justifies the observation that as the percentage weight fraction of Red mud increases, the hardness and compression strength of the total composite are also increases. Since finer particles are strongly bonded with each other in a composite, the hardness and compression strength values of the nano composites are higher when compared to the micro level.

Table: 5 Simulated results of Compressive Strength from Deform-2D software

S.No	%Wt of Red mud	Particle size μ m	Stress at 10% reduction MPa	Stress at 20% reduction MPa	Stress at 30% reduction MPa
1	Pure Aluminium	45	49.81	66.71	75.33
2	Aluminium + 2%RM	100	44.59	71.67	78.21
3	Aluminium +2% RM	0.042	46.12	72.95	79.57
4	Aluminium +4% RM	100	47.84	75.94	83.45
5	Aluminium +4% RM	0.042	59.36	74.21	86.42
6	Aluminium +6% RM	100	68.65	85.98	91.24
7	Aluminium +6% RM	0.042	54.95	89.54	95.74

3.2 Wear Rate

Experiments have been conducted on the Pin-on-disc Wear Testing machine with data acquisition system, which is used to evaluate the wear behavior of the composite, against hardened ground steel disc (En-32) having hardness 65 HRC and surface roughness (Ra) 0.5 µm. This equipment designed to study wear rate under sliding condition only. Sliding generally occurs between a stationary Pin and a rotating disc. The disc rotates with the help of a D.C. motor having speed range 0-1000 rpm with wear track diameter 50 mm-80 mm, which could yield sliding speed 0 to 10 m/sec. Load of 10N is to be applied on pin (specimen) by dead weight through pulley string arrangement. The wear tests are performed as per standards of ASTM G-99 with unlubricated condition in a normal laboratory atmosphere at 55% relative humidity and a temperature of 27-31ºC. Each Aluminium-Red mud composite samples are conducted for 6 hours. The samples are cleaned with the solution of tetra chloro ethylene before and after the wear test. In Table 6, the experimental wear rate results at 200, 400 and 600 rpm are shown.

From the figure 6 to figure 8 the results of Wear Rate Vs % Weight fraction of Red mud at 200, 400 and 600 rpm are plotted. The Red mud constituents (Ferrous oxide) are harder in nature, the percentage weight fraction of the red mud increases the wear resistance of the whole composite also increases. The maximum wear resistance is obtained for 42 nm or 0.042 microns level of 6% weight fraction of Red mud with Pure Aluminium.

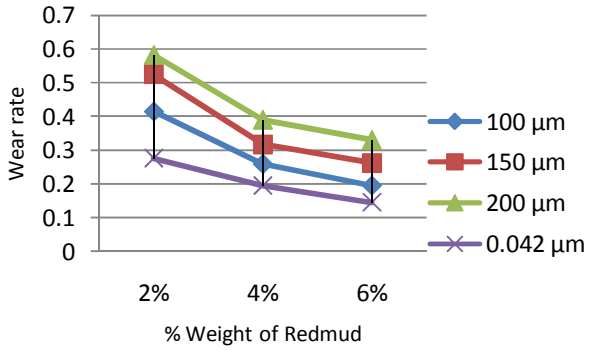

Figure 6: Plot between Wear Rate Vs %Weight fraction of Red mud at 200 rpm.

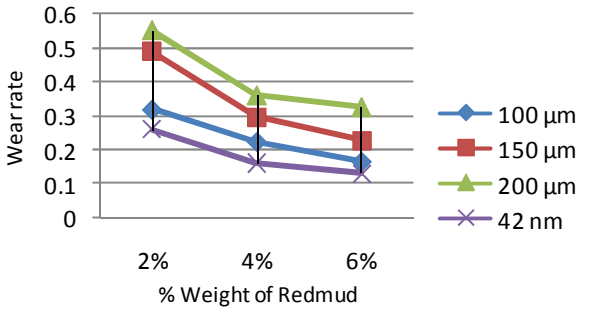

Figure 7: Plot between Wear Rate Vs % Weight fraction of Red mud at 400 rpm.

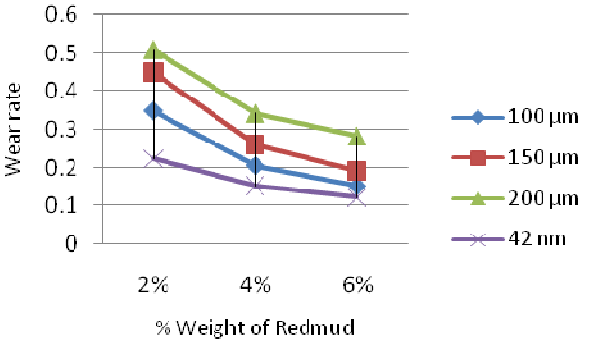

Figure 8: Plot between Wear Rate Vs % Weight fraction of Red mud at 600 rpm.

3.3 Mathematical Prediction

A mathematical model is developed and the overall equation is obtained using Regression analysis which is shown in equation 1. The multiple R value is 0.9554 and obtained standard error is 0.03928. The Overall equation is stated as below.

Wear rate = 0.434552+ [(0.001107) x particle size] - [(0.0519) x percentage Weight fraction of Red mud] - [(0.00013) x speed] (1)

Table 6: Experimental Results of Wear Rate from Pin-on-disc Wear Testing machine

S.No	Particle Size Microns	Wt % of Red mud gm	Speed RPM	Wear rate $X10^{-6}$N/m
1	100	2	200	0.415
2	150	2	200	0.524
3	200	2	200	0.582
4	0.042	2	200	0.276
5	100	4	200	0.259
6	150	4	200	0.317
7	200	4	200	0.39
8	0.042	4	200	0.195
9	100	6	200	0.195
10	150	6	200	0.262
11	200	6	200	0.33
12	0.042	6	200	0.145
13	100	2	400	0.391
14	150	2	400	0.488
15	200	2	400	0.553
16	0.042	2	400	0.259
17	100	4	400	0.224
18	150	4	400	0.295
19	200	4	400	0.36
20	0.042	4	400	0.162
21	100	6	400	0.165
22	150	6	400	0.228
23	200	6	400	0.325
24	0.042	6	400	0.131
25	100	2	600	0.35
26	150	2	600	0.45
27	200	2	600	0.51
28	0.042	2	600	0.223
29	100	4	600	0.207
30	150	4	600	0.261
31	200	4	600	0.342
32	0.042	4	600	0.152
33	100	6	600	0.153
34	150	6	600	0.192
35	200	6	600	0.282
36	0.042	6	600	0.122

The value of R square is 0.9128 and is very near to the unity i.e the relation between the weight percentageof red mud and the wear rate is linear, so the in between values can calculate with maximum accuratly.

4.0 CONCLUSION

An increase in hardness and compression strength is observed with increase in the amount of percentage weight fraction of Red mud. It is also observed that, for the same percentage weight fraction of Red mud, the hardness and compression strength are higher for the nano structured reinforcement than micro structured reinforcement. This is due to the increase in surface area of contact and higher bond strengths. Hardness and compression strength properties are improved for nano level

Aluminium-Red mud test specimen with 42 nm size and 6% weight fraction of Red mud. The Simulated results of Compression Strength using Deform-2D software and experimental values are within the limits of 2-5% difference. As increase in speed of rotation of the specimen, the wear resistance is higher. Highest wear resistance is observed for the test specimen with 42 nm size and 6% weight fraction of Red mud powder at 600 RPM speed.

ACKNOWLEDGEMENTS

The Corresponding author wish to express her sincere gratitude to Prof.N.Selvaraj, NIT Warangal and Prof.V.Mahesh S.R Engineering College,Warangal.

REFERENCE

1. Mondal, D.P., Das, S., Nidhi Jha. (2009). *Dry sliding wear behavior of aluminum syntactic foam*, Mater Des Vol. 30, pp: 2563–2568.
2. Yang, Y., Li, X. (2004). *Study on bulk aluminium matrix Nano-composite fabricated by ultra-sonic dispersion on Nano sized SiC particles in molten aluminium alloy*, Materials Science and Engineering-A Vol. 38, pp: 378-383.
3. Unlu, B.S. (2008). *Investigation of tribological and mechanical properties Al_2O_3-SiC reinforced Al composites manufactured by casting or P/M method*, Materials and Design Vol. 29(10), pp: 2002–2008.
4. John, E Allison., Gerald, S Cole. (1993). *Metal Matrix Composites on the automotive Industry Opportunities and Challenge*, JOM Vol. 45(1), pp: 19-24.
5. Rao, R.N., Das, S., Mondal, D.P., Dixit, G. (2009). *Dry sliding wear behavior of cast high strength aluminium alloy (Al–Zn–Mg) and hard particle composites*, Wear Vol. 267, pp: 1688–1695.
6. Ghazali, M.J., Rainforth, W.M., Jones, H. (2007). *The wear of wrought aluminium alloys under dry sliding conditions*, Tribol Int Vol. 40, pp: 160–169.
7. Sharma, S.C. (2001). *The sliding wear behavior of Al6061–garnet particulate composites*, Wear Vol. 249, pp: 1036–1045.
8. Liu, W., Zhang, X., Jiang, W. (2011). *Study on particle-size separation pretreatment of Bayer red mud*, J. Environ. Eng Vol. 5, pp: 921–924.
9. Han, Y., Yang, Y., Wang, X. (2011). *Research on the basic characteristics and utilization value of the Sintering process and Bayer red mud*, Mater Rev Vol. 25, pp: 122–126.
10. Deuis, R.L., Subramanian, C., Yellup, J.M. (1996). *Abrasive wear of Aluminium composites- a review*, Wear Vol. 201, pp: 132-144.
11. Rahimian, M., Parvin, N., Ehsani. N. (2011). *The effect of pro-diction parameters on microstructure and wear resistance of powder metallurgy Al-Al_2O_3 composite*, Materials and Design Vol. 32, pp: 1031-1038.
12. Wilson, S., Alpas, A.T. (1997). *Wear mechanism maps for metal matrix composites*, Wear Vol. 212, pp: 41–49.
13. Sharma, S.C. (2001). *The sliding wear behavior of Al6061–garnet particulate composites*, Wear Vol. 249, pp: 1036 – 1045.
14. Ghazali, M.J., Rainforth, W.M., Jones, H. (2007). *The wear of wrought aluminium alloys under dry sliding conditions*, Tribol Int Vol. 40, pp: 160–169.
15. Paramguru, R.K., Rath, P.C., Misra, V.N. (2005). *Trends in red mud utilization—A review*, Miner Process Extr Metall Rev, Vol. 26, pp: 1–29.

Journal of Ocean, Mechanical and Aerospace
-Science and Engineering-, Vol.25

November 30, 2015

Hydrodynamic Effects of the Length and Angle of the Ducted Propeller

Sohrab Majdfar[a], Hassan Ghassemi,[b,*], and Hamid Forouzan[c]

[a,c] *Department of Marine Engineering, Imam Khomeini University, Nowshahr,, Iran.*
[b] *Department of Maritime Engineering, Amirkabir University of Technology, Tehran, Iran.*

*Corresponding author: gasemi@aut.ac.ir

Paper History

Received: 14-November-2015
Received in revised form: 27-November-2015
Accepted: 30-November-2015

ABSTRACT

Ducted propellers used in many vessels, especially fishing vessels, trawlers and submarine which provide the higher efficiency. In this article, the effects of the duct length and duct angle are investigated on the hydrodynamic performance. First, did the modeling of duct 19A. The Kaplan propeller performance with nozzle 19A by turbulence model of SST-K-ω analyzed and validated with experimental results that indicate acceptable accuracy. Finally, by changing the nozzle at a rate of 10% and 20% of the original length of the nozzle and also change the angle of the nozzle, analyzed the effects of the changes made. The Kaplan propeller with 19A nozzle is selected for case study. A Reynolds Average Navier-Stokes (RANS) turbulence model of the SST-K-ω employed for the present calculations. Numerical results are included pressure distribution, hydrodynamic characteristics and velocity behind the propeller at various geometry and physical conditions. Comparisons of the results are shown with acceptable agreement by the experimental data. It is concluded that the position of the propeller and increasing the duct angle inside the duct may be limited.

KEY WORDS: *Ducted propeller, RANS, Hydrodynamic Characteristics.*

NOMENCLATURE

API	American Petroleum Institute
ΔT	Temperature Difference in and out
F_T	Thermal Expansion
L_A	Anchor Length
ΔL	Expansion
F_P	Pressure Force
F_F	Friction Force
ε_{sd}	Design Compressive Strain
ε_c	Critical Strain

1.0 INTRODUCTION

Ducted propellers consist of a combination of two principal components. The first is an annular wing which can be either symmetric with respect to the rotation axis or asymmetric to accommodate for the wake flow field variations. The second component, i.e. the propeller, differs from a typical open propeller because it has to be designed taking into account the mutual interaction between the duct and the rotor. In general, there are two main types of ducts: the accelerating (also called the Kort Nozzle) and the decelerating duct (also referred to as pumpjet that Stipa [1] and Kort [2] experimentally proved the increase of the efficiency which can be obtained by ducting the propeller with an accelerating nozzle.

The ability to accurately predict the thrust and torque of a ducted propeller in open-water conditions is very important for a calculation method used in the design stage. The RANSE methods have been progressively introduced for the calculation of ducted propeller systems, meeting considerable success in predicting open-water characteristics for the well-known Ka-series (Sanchez-Caja et al [3]), (Abdel-Maksoud & Jeinke [4]) and (Krasilnikov et al [5]). However, due to their relative complexity and time requirements, they are not yet routinely used in the design process, which is often still based on the use of inviscid flow methods. Krasilnikov studied mesh generation techniques for the Analysis of ducted propellers using a commercial RANSE solver and its application to scale effect.

Various numerical methods based on inviscid (potential) flow theory have been proposed for the analysis of ducted propellers. For example: Kerwin et al [6] used combination of a panel method, also known as boundary element method (BEM), to model the duct with a vortex lattice method for the propeller, and Lee and Kinnas [7] used a panel method for the complete ducted propeller system operating in unsteady flow conditions including blade sheet cavitations. Both methods applied a transpiration velocity model for the gap flow between propeller blade tip and duct inner surface, and analyzed duct with a sharp trailing edge. The sources indicate that the use of non-viscous flow model to ducted propeller, with its many benefits, there may be some serious limitations in the areas of flow where viscosity effects cannot be ignored to meet and should be modeled for the correct prediction of thrust and torque of ducted propeller. One of such region concerns the gap flow, which has a strong influence on the propeller and duct circulation distribution, and therefore, on the distribution of loading between propeller and duct, as studied in detail by Baltazar & Falcão [8]. In addition, there may be a considerable interaction between the vortices shed from the propeller blade tips and the boundary layer developing on the duct inner side, as found in the works of Krasilnikov et al and Rijpkema & Vaz [9]. This effect has not been studied before with potential flow methods and its importance is therefore unknown. Ducted propeller was also done in the field of design. Bobo et al [10] design of ducted propeller and model tests of a fishing research vessel for M.Cies Shipyards. Hughes [11] and Moon et al [12] presented a specific method to model the flow between the inner plate of nozzle and propeller tip. Falco and Campos [13] studied on the calculation of ducted propeller performance in axisymmetric flows. Hoekstra [14] presented a RANS-based analysis tool for ducted propeller systems in open water conditions. Zondervan, Hoekstra and Holtrop [15] researched on the flow analysis, design and model testing of ducted propellers. Gu & Kinnas [16] modeled the flow around a ducted propeller by a vortex lattice and finite volume methods. Haimov et al [17] research on ducted propellers as better propulsion of ship by calculations and practices. Baltazar et al [18] studied on open water thrust and torque predictions of a ducted propeller system with a panel method. An experimental and numerical study on wake vortex noise of a low speed propeller fan carried out by Sasaki et al [19]. A series work based on both potential method and RANSE solver for the whole geometry have been done for a multi-component linear jet optimization by Abdel- Maksoud et al [19] and Steden M et al [20]. In this study, we are trying to show that there are some numerical analysis software to predict and investigate of propellers, and with validation of one of them, the effects of changes on duct want to study on ducted propeller.

2.0 GEOMETRIC MODELING

The most common propeller for ducted propellers is Kaplan type. The Ka 4-70 propeller comes from the famous Wageningen propeller series. It is a traditional ducted propeller that has a large chord at the tip. For all results in this paper the Kaplan propeller with a P/D ratio of 0.8 is used. Geometric modeling of Kaplan propeller is done by Propcad and Solidworks software's that Kaplan geometric data and Nozzle is shown in Table 1.

Table 1: Kaplan geometric parameters and nozzle characteristics

Parameter	Value
Prop. Dia.	Dp=300mm
Number of blades	Z=4
Pitch ratio	P/D=0.8
Expanded Area Ratio	EAR=0.70
Nozzle length	L=0.5DP
Nozzle type	19A

The 19A and 37 nozzles are the most common type of nozzles due to the favorable hydrodynamic properties. In this article the 19A nozzle applied which is an accelerator nozzle. The nozzle length is equal to half of propeller diameter and the distance between the propeller tip and the inner surface of the nozzle is equal to one percent of propeller diameter (3 mm).
We found the nozzle data and made it in the Solidworks that shown in Figure 1. Then assembled duct and propeller are shown in Figure 2.

3.0 MESH GENERATION AND BOUNDARY CONDITIONS

After Modeling of ducted propeller and domains, divided it into 4 pieces and applied one piece with smaller cells because of higher accuracy in calculations.

The computational domain consists of an internal rotating cylinder containing the propeller and an external stationary cylinder with radius 1.5D. The inlet uniform boundary condition is located at 3D upstream of the propeller plane and the constant pressure condition is imposed 6.5D downstream that shown in Figure 3. At the inlet of the cylinder the velocity is prescribed and at the outlet the pressure. For a thrust producing operating condition of the propeller, the fluid through the duct is accelerated. Then ICEM meshing tools applied.

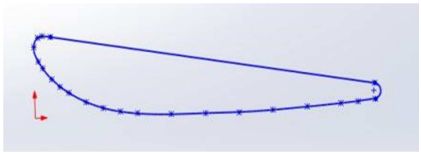

Figure 1: Section of duct in Solidworks

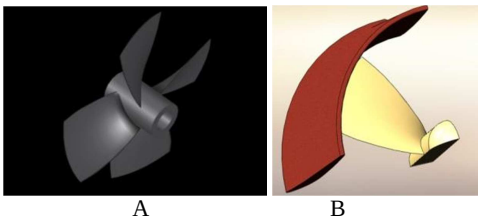

A B

Figure 2: A) 3D model of Kaplan propeller B) ducted propeller Assembled in Solidworks

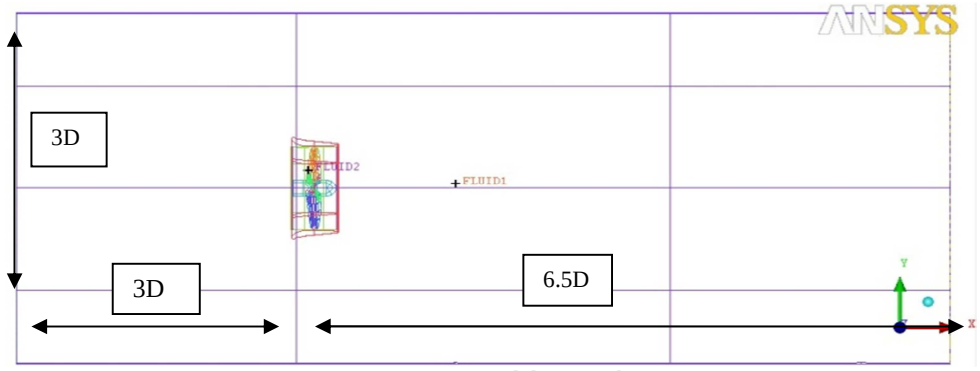

Figure 3: Computational domains dimensions

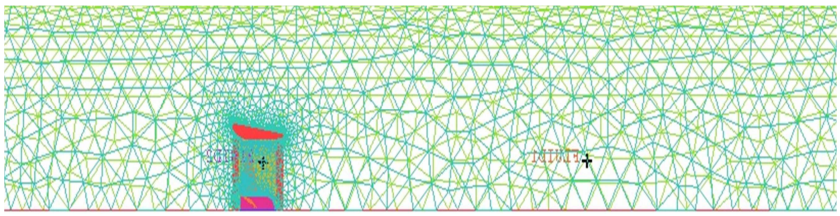
Figure 4: Division of calculation domain with mesh

In this analysis, the rotational velocity of the propeller is imposed by a moving reference frame (MRF) applied to the inner region of the domain because of low time in computation and acceptable accuracy in simulation. All domains divided into two sections: 1- main domain that is stationary domain with larger mesh 2- rotating domain with small mesh around propeller that shown in Figure 4.

The generated mesh size grows outwards with ratio 1.2 then defined boundary conditions that include inlet, outlet, rotating domain, open water, propeller and duct that Figure 5 shown meshes near of propeller and duct. First mesh with 1 million mesh used for model then smaller mesh used with 1.4, 1.5 and 1.7 millions cells and the results at advanced ratio of 0.4 compared. Comparison of results showed that minimum number of cells for this model is 1.4 millions and Figure 6 showed independence of results from meshes.

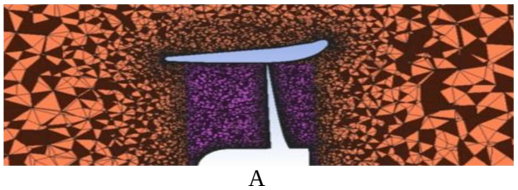
A

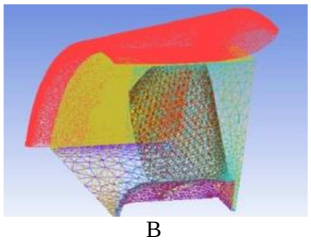
B

Figure 5: A, B) Mesh cells on the propeller and duct

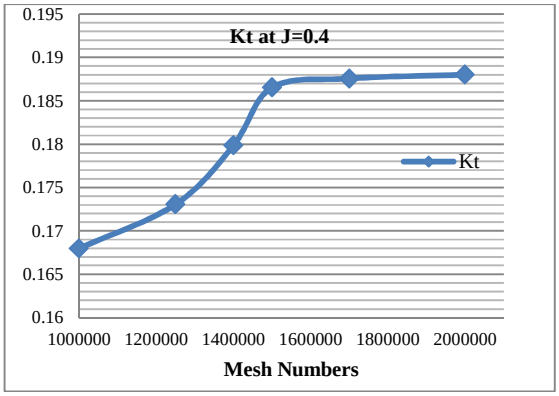

Figure 6: Independence of results from meshes

4.0 SOLVER SETTINGS

The CFD code applied is ANSYS CFX v.14. The Reynolds Averaged Navier-Stokes equations are solved numerically by a finite volume technique. High Resolution method used to discrete equations and first order method used for investigate of turbulence. SST model selected for turbulence because applied in most of the articles due to higher accuracy. 3000 iterations selected in determining the number of iteration to achieve convergence and the remaining amount is considered 0.0001.

5.0 VALIDATION

After completion of solver module, numerical results compared with experimental results to validate software. The experimental results of model tests normally present values of K_T, K_Q and

Efficiency plotted as a function of advance coefficient J for a fixed pitch ducted propulsor as shown in Marine Propellers and Propulsion book [21]. The software outputs were thrust coefficient, torque coefficient and efficiency that obtained by thrust and torque of propeller and duct. The equations 1-4 have shown method to calculate hydrodynamics performance of propeller in different advance coefficients.

$$advanced\ coefficient: \quad J = \frac{V_A}{nD} \qquad (1)$$

$$Thrust\ Coefficient: \quad K_T = \frac{T}{\rho n^2 D^4} \qquad (2)$$

$$Torque\ Coefficient: \quad K_Q = \frac{Q}{\rho n^2 D^5} \qquad (3)$$

$$Efficiency: \quad \eta = \frac{K_T}{K_Q} \times \frac{J}{2\pi} \qquad (4)$$

where V_A is advanced velocity, n is angular velocity, D is Propeller Diameter, T is total thrust, ρ is water density and Q is total torque. Comparison of the numerical and experimental data is shown in Fig. 7. The relative error is about less than 10%. Also the pressure contours on front and back of propeller at advanced ratio 0.3 is shown in Fig. 8. The blade tip is located where the pressure lines converge. On the suction side of the blade tip a low pressure area can be observed.

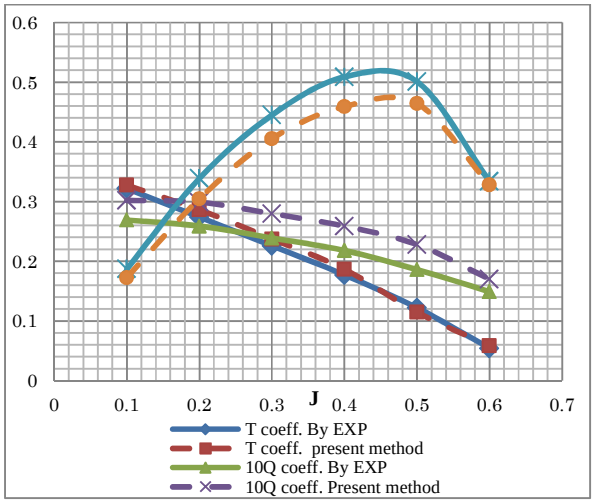

Figure 7: Comparison of the numerical and experimental hydrodynamics characteristics of ducted propeller

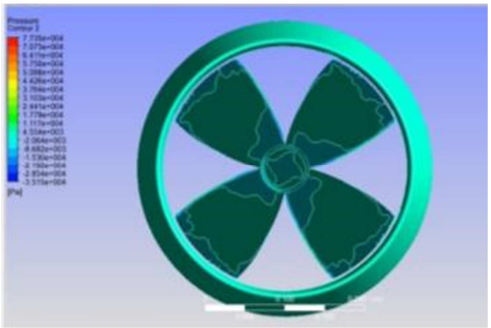

A

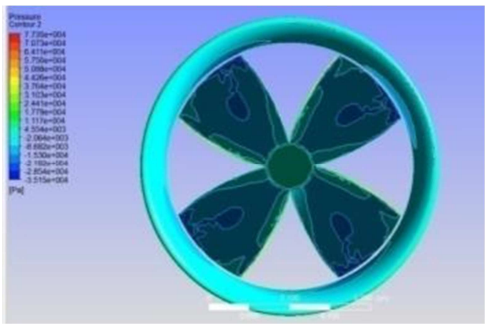

B

Figure 8: A: Pressure contours on back and B: face of ducted propeller at J=0.3

6.0 RESULTS

6.1 Increase the Nozzle Length

After validation of the software, 3D models of duct with 10 and 20 percent of first duct length created in Solidworks. Then save it with IGES format and import to ICEM for meshing with same settings of the original model. Then specify boundaries settings of model in Ansys CFX-pre and run solver to export the results. It should be noted that all nozzle types are 19A.

To examine the effect of increasing the length of the nozzle, numerical results obtained for the first model. Fig. 10 illustrates comparison of ducted propeller with increase of 10%duct length and standard length. In all advanced ratios, increasing of length showed higher efficiency about 2% and it shows positive effect on hydrodynamics characteristics of ducted propeller. Fig. 9A show the velocity vectors in case of increased length 10% at J=0.3 and Fig. 9B showed velocity contours. Fig. 11 illustrates pressure distribution on blade at various radiuses. The sudden pressure jump at the blade tip (x=0) is clearly visible. Some oscillation showed at leading edge but at chord length showed uniform distribution of pressure on blade. Fig. 12 showed pressure distribution on duct with increasing of length 10%.

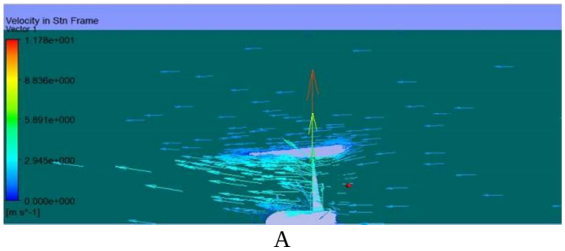

A

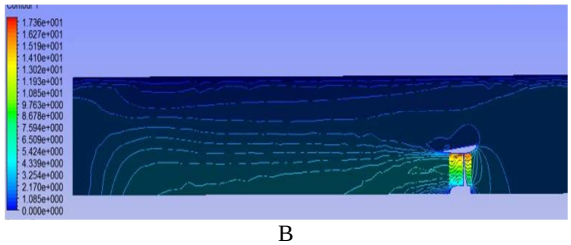

B

Figure 9: A: Velocity vectors B: Velocity contours in 10% increase length at J=0.3

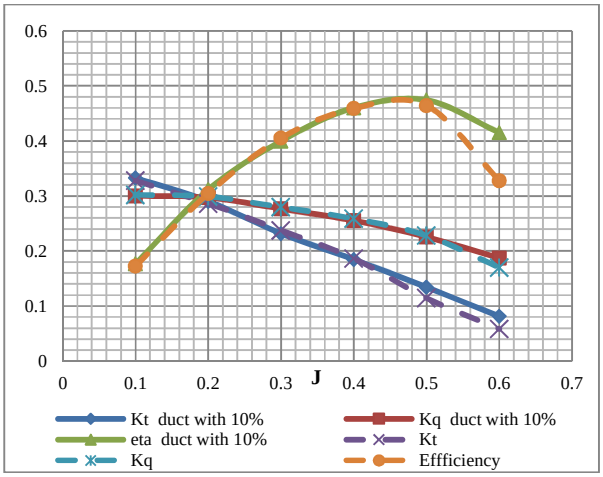

Figure 10: Comparison of the hydrodynamics characteristics of ducted propeller

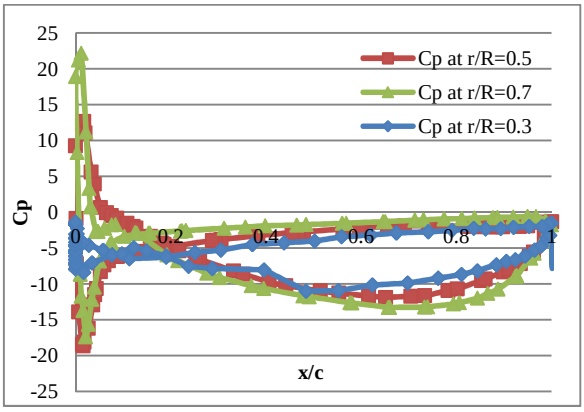

Figure 11: Pressure distributions on propeller at different radiuses in propeller with 10% increasing of duct length

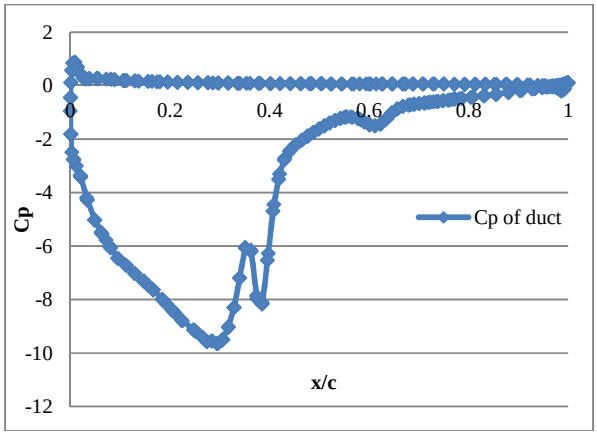

Figure 12: Pressure distributions on duct with 10% increasing of duct length

The numerical results obtained from increasing duct length 20% compared with first model have shown in Fig. 14. As can be seen, increase 20% length of duct had negative effect on the performance of propeller and nozzle, which reduces the coefficient values of thrust, torque and efficiency in comparison with increase of 10% of length. In this case study, increase of length caused to increase about 1.6% of efficiency. Fig. 13A and 13B show velocity vectors and contours in case of 20% increase of length at advanced ratio 0.3 that show decrease in values.

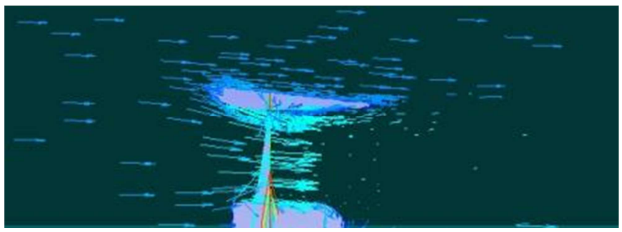

A

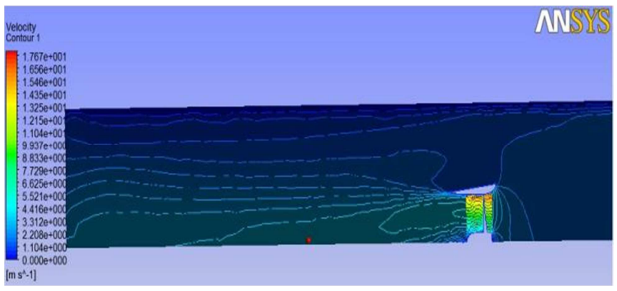

B

Figure 13: A: Velocity vectors and B: Velocity contours in 20% increase length at J=0.3

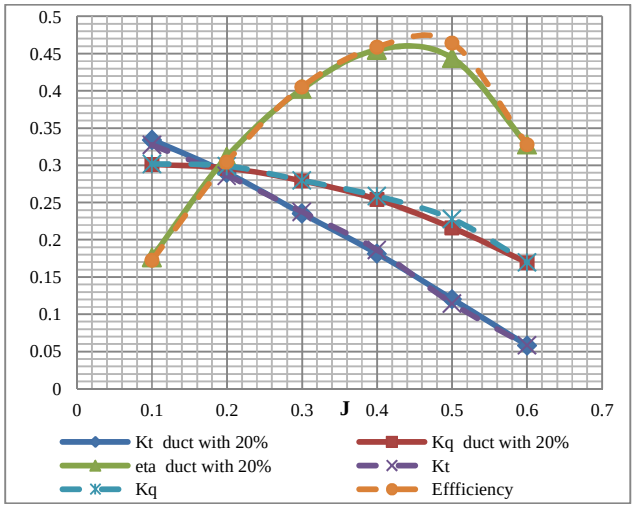

Figure 14: Comparison of the numerical and experimental hydrodynamics characteristics of ducted propeller

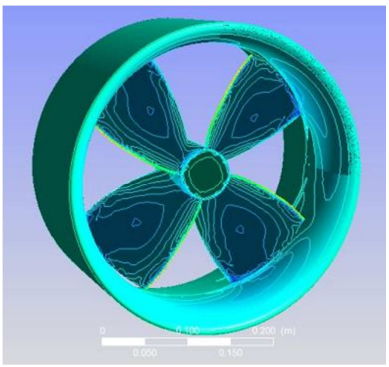

A

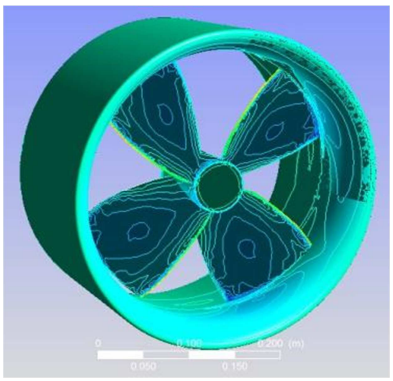

B

Figure 15: A: Pressure contours in ducted propeller with 10% increase of length B: pressure contours in ducted propeller with 20% increase of length

Fig. 15 shows the difference between pressure contours distribution on front side of propeller and nozzle in cases of increasing in duct length. Lower pressure is observed in model with 20% increase of length. Also Fig. 16 shows uniform pressure distribution on blade and some oscillation at leading edge but the amount of pressure has small decrease in compared with previous case study. Fig. 17 shows pressure distribution on duct with increase 10% of length that has less oscillation.

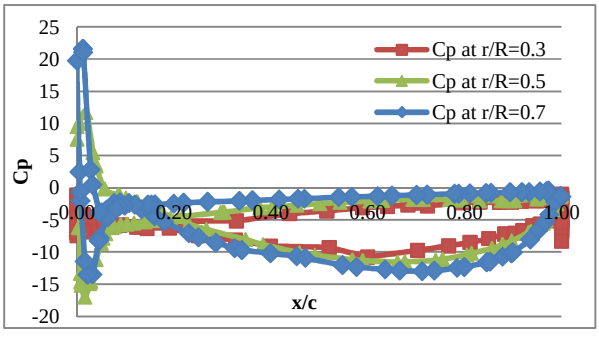

Figure 16: Pressure distributions on propeller at different radiuses in propeller with 20% increasing of duct length

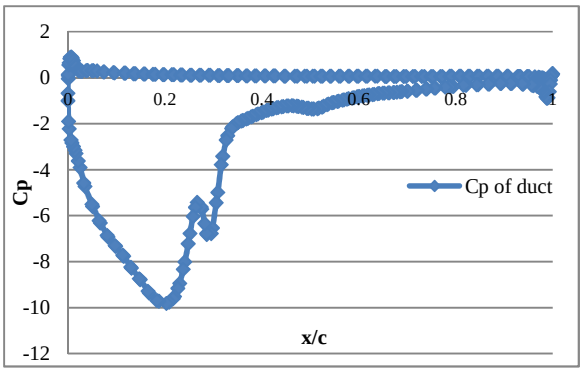

Figure 17: Pressure distributions on duct with 20% increasing of duct length

7.2 Model with Duct Angle 10 Degree

Now, for investigate the effect of increase in duct angle, change the model of duct. After modeling of new duct specified boundaries settings and run solver module to export results for different advanced ratios. The results compared with first model in Fig. 18. Increase in duct angle causes to increase thrust and torque coefficients that more effect of this change is showed at lower advanced ratios. In heavy conditions for this model, the thrust is more than first model but effect on torque is more than thrust and causes to decrease total efficiency of ducted propeller.

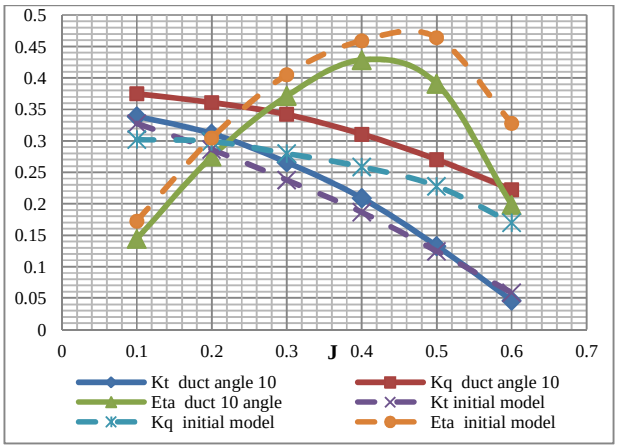

Figure 18: Comparison of hydrodynamics characteristics of the ducted propeller in cases normal duct and duct with 10 degree duct angle

7.0 CONCLUSION

In this paper, the Kaplan propeller with nozzles 19A analyzed by numerical method and the following results are concluded:

- ✓ Pressure coefficient distribution on the duct and blade are presented in contours and diagram. Negative low pressure coefficients are shown in back side and high pressure is given in face side of the blade. On the duct is also shown low pressure at suction side (mean inside the duct).

- ✓ To evaluate the effect of increasing the duct length on the performance of the propeller in open water, the nozzle section length increased to 10 and 20 percent. The results show that increasing 10% of the nozzle length has positive effect on the performance of the propeller but increase the nozzle length further 10% will have a negative effect on propeller performance.
- ✓ Effect of the duct angle up to 10 degree and the results are compared with the first model results. It is shown that with increasing duct angle the thrust and torque of propeller are also increased but the efficiency is diminished.

REFERENCE

1. Stipa, L. (1931). *Ala a turbina*. L'Aerotecnica, 923–953.
2. Kort, L. Der neue d. (1934).¨*usenschrauben-antrieb*. Werft, Reederei und Hafen, 15.
3. Sanchez-Caja, A., Rautaheimo, P. & Siikonen, T.(2000). *Simulation of incompressible viscous flow around a ducted propeller using a RANS equation solver*. Proceedings of the Twenty-Third Symposium on Naval Hydrodynamics,.
4. Abdel-Maksoud, M. & Heinke, H.-J. (2003). *Scale effects on ducted propellers*. Proceedings of the Twenty-Fourth Symposium on Naval Hydrodynamics, Fukuoka, Japan.
5. Krasilnikov, V. I., Sun, J. Y., Zhang, Z. & Hong, F. (2007). *Mesh Generation Technique for the Analysis of Ducted Propellers Using a Commercial RANSE Solver and its Application to Scale Effect Study*. Proceedings of the 10th Numerical Towing Tank Symposium (NuTTS'07).
6. Kerwin, J. E., Kinnas, S. A., Lee, J.-T. & Shih, W.-Z. (1987). *A surface panel method for the hydrodynamic analysis of ducted propellers*. Transactions of Society of Naval Architects and Marine Engineers 95.
7. Lee, H. & Kinnas, S. A. (2006). *Prediction of cavitating performance of ducted propellers*. Proceedings of the Sixth International Symposium on Cavitations.
8. Baltazar, J. &Falcão de Campos, J. A. C. (2009). *On the modeling of the flow in ducted propellers with a panel method*. Proceedings of the First International Symposium on Marine Propulsors, Trondheim, Norway.
9. Rijpkema, D. &Vaz, G. (2011). *Viscous Flow Computations on Propulsors: Verification, Validation and Scale Effects*. Proceedings of the Developments in Marine CFD.
10. Bobo M. J., De La Rosa J.-C., Masip J., Quereda R. & Pangusión, L. (2005). *Design of ducted propeller and model tests of a fishing research vessel for M.Cies Shipyards*. OTI 2233-2, CEHIPAR (in Spanish).
11. Hughes, M. J. (1997), *Implementation of a special procedure for modeling the tip clearance flow in a panel method for ducted propellers*. Proceedings of the Propellers/Shafting '97 Symposium.
12. Moon, I.-S., Kim, K.-S., and Lee, C.-S. (2002). *Blade tip gap flow model for performance analysis of waterjet propulsors*. In International Association for Boundary Element Methods, Austin, Texas, USA.
13. Falcao de Campos, J. A. C. (1983). *On the calculation of ducted propeller performance in axisymmetric flows.* PhD Thesis, Delft University, Wageningen, the Netherlands.
14. Hoekstra, M. (2006). *A RANS-based analysis tool for ducted propeller systems in open water conditions*. International Shipbuilding Progress 53, 205-227.
15. Zondervan, G-J., Hoekstra, M. & Holtrop, J. (2006). *'Flow Analysis, Design and Testing of Ducted Propellers.* Proceedings of Propeller/Shafting Symposium, Virginia Beach, United States.
16. Gu H and Kinnas S A. (2003). *Modeling of contra-rotating and ducted propellers via coupling of a vortex-lattice with a finite volume method*. In: Proceedings of Propeller/Shafting Symposium, SNAME, Virginia Beach, USA.
17. Haimov, H., Bobo, M.J., Vicario, J. & Del Corral, J. (2010). *Ducted propellers. A Solution for Better Propulsion of Ships. Calculations and Practice*. Proceedings of First International Symposium on Fishing Vessel Energy Efficiency, Vigo, Spain.
18. J. Baltazar, J.A.C. Falcão de Campos and J. Bosschers (2011). *Open-Water Thrust and Torque Predictions of a Ducted Propeller System with a Panel Method*, Second International Symposium on Marine Propulsors smp'11, Hamburg, Germany, June.
19. Sasaki S., Torise I., Hayashi H. (2012). *An experimental and numerical study on wake vortex noise of a low speed propeller fan*, Open Journal of Fluid Dynamics, 2, 290-296.
20. Abdel-Maksoud M, Steden M and Hundemer J. (2010). *Design of a Multi-Component Propulsor*. In: Proceedings of 28th Symposium on Naval Hydrodynamics, Pasadena, USA, September.
21. Steden M, Hundemer J, Abdel-Maksoud, M, (2009). *Optimization of a linearjet*, First International Symposium on Marine Propulsors, Trondheim, Norway.
22. Carlton, J. S. *"Marine Propellers and Propulsion"*, 3rd edition, 2012

Publishing

ISOMAse
Resty Menara Hotel
Jalan Sisingamangaraja No.89
Pekanbaru-Riau, INDONESIA
http://www.isomase.org/

Editing

Building P-23, Room: 314
Department of Aeronautics,
Automotive & Ocean Engineering,
Faculty of Mechanical, Universiti
Teknologi Malaysia, MALAYSIA
http://web1.fkm.utm.my/

ISSN: 2354-7065

Publication

Teknik Mesin
Fakultas Teknik,
Universitas Riau, INDONESIA
http://www.unri.ac.id/en

Organizing

Ocean & Aerospace Research
Institute, Indonesia
Pekanbaru-Riau, INDONESIA
http://isomase.org/OCARI.php/

Supporting

Mechanical Chapter of the
Institution of Engineers,
INDONESIA

Malaysian Joint Branch Royal
Institution of Naval Architects &
Institute of Marine Engineering,
Science and Technology
-Southern Chapter (MJB RINA
&IMarEST – SC)-